Andreev Reflection of Helical Edge Modes in InAs/GaSb Quantum Spin Hall Insulator

Ivan Knez, Rui-Rui Du, and Gerard Sullivan

Phys. Rev. Lett. **109**, 186603 — Published 31 October 2012

DOI: 10.1103/PhysRevLett.109.186603

Andreev Reflection of Helical Edge Modes in InAs/GaSb Quantum Spin Hall Insulator

Ivan Knez* and Rui-Rui Du**

Department of Physics and Astronomy, Rice University, Houston, TX 77251-1892

Gerard Sullivan

Teledyne Scientific and Imaging, Thousand Oaks, CA 91630

ABSTRACT

We present an experimental study of S-N-S junctions, with N being a quantum spin Hall insulator made of InAs/GaSb. A front gate is used to vary the Fermi level into the mini-gap, where helical edge modes exist [Phys. Rev. Lett., 107, 136603 (2011)]. In this regime we observe a ~ $2e^2/h$ Andreev conductance peak, consistent with a perfect Andreev reflection on the helical edge modes predicted by theories. The peak diminishes under a small applied magnetic field due to the breaking of time-reversal symmetry. This work thus demonstrates the helical property of the edge modes in a quantum spin Hall insulator.

Quantum Spin Hall Insulator (QSHI) is a two-dimensional version of a novel class of materials characterized by topological order, whose unique properties have recently triggered much interest and excitement in the condensed matter community. [1, 2] Most notably, topological properties of these systems hold great promise in mitigating the difficult problem of decoherence in implementations of quantum computers. [3] Although QSHI has been theoretically predicted in a few different materials, [4, 5, 6, 7] so far only the semiconductor systems of HgTe/CdTe [8] and, more recently, inverted InAs/GaSb, [9] have shown experimental evidence for the existence of this phase. While insulating in the bulk, QSHI is characterized by one-dimensional channels at the sample perimeter, which have helical property, with carrier spin tied to the carrier direction of motion, and protected from back-scattering by time-reversal symmetry. Much of the transport phenomenology of QSHI has been established in a set of remarkable experiments in HgTe material system, [8, 10] including the quantized conductance and the non-local character of the QSH edge modes. Combining QSHI with superconductors is the next experimental challenge, posing fundamental questions regarding the nature of topological superconductors and the possible realizations of Majorana fermion bound states. [3, 11, 12, 13] Recently it has been theoretically suggested that Andreev reflection (AR) can be used as a powerful method to probe helical edge modes, where a perfect Andreev reflection should be observed even in the presence of a finite potential barrier and nonmagnetic disorders. [14, 15] InAs/GaSb material systems is well suited for the task, due to its low Schottky barrier and good interface to superconductors. [16, 17, 18]

In this Letter, we study novel electrical transport in inverted InAs/GaSb quantum wells (QWs) in hybridization regime, where helical edge modes have been recently reported. [9] In this case, structures are contacted by superconducting niobium electrodes. We observe strong zero-

bias conductance peaks (ZBCP) as the Fermi level is tuned across the hybridization gap via a front gate. Analysis of the relative amplitude of the peaks and the corresponding excess current is in agreement with expectations of perfect Andreev reflection of the helical edge modes, validating their helical property and topological protection from back-scattering. Excess current and ZBCP show only weak temperature dependence for temperatures lower than the critical temperature of the superconducting electrodes. On the other hand, weak magnetic field of less than 50 mT is sufficient to completely suppress the excess current in the hybridization gap, indicating a strong sensitivity to time-reversal breaking.

The experiments are performed on high quality 12.5 nm InAs/5 nm GaSb QWs, patterned in a superconductor-normal metal-superconductor (S-N-S) junction geometry. Sample structure is shown in Fig. 1 inset a). Electron and hole two-dimensional gases are situated in InAs and GaSb layers respectively, and confined by AlSb barriers. In the inverted regime, the electron subband is lower than the hole subband leading to band anti-crossing and mini-gap opening. [19, 20, 21] Energy spectrum with the resulting hybridization gap is shown in Fig. 1 inset b). Due to the band inversion, helical edges modes appear in the mini-gap. [7] In order to probe the helical character of the edge modes, superconducting niobium electrodes with a critical temperature of T_c = 8.27 K (BCS gap of Δ_S =1.24 meV) are deposited directly on InAs layers via magnetron sputtering. Top layers of the contact region are selectively removed by etching, and plasma cleaned in argon atmosphere *in-situ* prior to niobium deposition. [16, 17, 18] The width and length of the junctions are $W \sim 1$ μm and L ~ 0.5 μm. The front gate is fabricated by depositing Si_3N_4 using a plasma enhanced chemical vapor deposition system, followed by evaporating Ti/Au metal gate. Additional sample and processing details are given elsewhere. [9, 21]

Andreev reflection [22] is a process unique to the S-N interface, where impinging normal quasiparticle retroreflects, having thus not only opposite velocity but also opposite charge, and resulting in the enhancement of the total current across the interface. The electrical current through a single S-N interface can be calculated using the Blonder-Tinkham-Klapwijk (BTK) model [23]:

$$I = \frac{N \cdot e}{h} \int \left[f(E + eV) - f(E) \right] \cdot \left[1 + A(E) - B(E) \right] \cdot dE \quad , \qquad (1)$$

where N is the number of modes in the normal conductor, $f(E)$ is the equilibrium Fermi distribution function, V is the voltage drop at the interface, and $A(E)$ and $B(E)$ are probabilities for Andreev and normal reflection (NR) of the electron at the interface. In the case of ideal interface, and for biases within the superconducting gap ($V < \Delta_S/e$), quasi-particles are only Andreev reflected. This is because transmission is prohibited within the superconductive gap, and there is no potential barrier which would absorb momentum difference necessary for normal reflection (NR). In practice, due to native oxides or Schottky barriers, a potential step always exists at the S-N interface, allowing for normal reflection and hence reducing the probability for Andreev reflection. The interface barrier is characterized by the scattering parameter Z which is related to the normal transmission of the barrier as: $T = \frac{1}{1+Z^2}$. For $Z < 1$, Andreev reflection dominates over normal reflection resulting in zero bias peaks in differential conductance dI/dV. In this case, current enhancement due to Andreev reflection manifests as an excess current I_{excess}, which is obtained by extrapolating linear I-V curve at high biases, i.e. for $V >> \Delta_S/e$, to zero bias[24].

Fig. 1 shows dV/dI verses bias voltage V across the S-InAs/GaSb-S junction, at different front gate bias V_{front}. Regime of interest to current work, i.e. center of the mini-gap regime occurs

at front gate bias of V_{front} =-2.1V. At a positive bias (e.g., V_{front} = 5V) , the Fermi level E_F of InAs/GaSb is on the electron side. As the E_F is tuned into the mini-gap, *dV/dI* exhibits a strong peak at larger biases, *i.e.* for $V >> \Delta_S/e$ (e.g., V at $\pm$5meV). On the other hand, for V tuned towards zero $(< \Delta_S/e)$, *dV/dI* exhibits a strong dip, *i.e.* enhanced conduction due to AR. Fig. 2a shows normal resistance R_N, *i.e. dV/dI* for $V >> \Delta_S/e$, verses V_{front} (in blue) and I_{excess} vs. V_{front} (in red). As E_F is tuned towards the mini-gap, R_N increases towards a peak value of ~ 2 kΩ, while concurrently I_{excess} decreases from the maximal value of ~ 2.6 μA to the mini-gap value, with an I_{excess} fluctuating around ~ 150 nA. Using the resistance data from Fig. 1 we calculate excess conductance $\Delta G \equiv G(V=0) - G(V >> \Delta_S / e)$, and plot ΔG verses V_{front} on a log scale, in Fig. 2b. We note that such subtraction procedure entails an error estimated to be $\pm 20\%$. For E_F in the mini-gap ΔG fluctuates around ~ 2.2 e^2/h, a value that is close to $2e^2/h$ predicted for helical edge channels.

We now analyze the non-linear conductance observed in the usual metallic and the QSH regime, respectively. In Fig. 2c we plot *I-V* and *dI/dV-V* curves for V_{front} = 5V. In this case E_F is high above the hybridization gap, and a ZBCP is observed indicating strong AR. Extrapolating current from high biases gives I_{excess} ~ 2.6 μA. The scattering parameter of the barrier can be estimated from the ratio $\frac{e \cdot I_{excess} \cdot R_N}{\Delta_S}$ ~ 0.76, [24, 25] to give Z = 0.65 and a normal transmissivity of T = 0.7. This transmissivity is only slightly lower than the largest reported value of 0.86 for the InAs material system. [18] In spite of a high transmissivity, the absence of supercurrent in our structures suggests that coherence is not preserved across the junction, presumably due to the surface degradation during plasma cleaning. Nevertheless, this simplifies the analysis in the case when E_F is in the mini-gap, allowing us to add conductance contributions from each S-QSH interface independently, as previously done in N-QSH-N structures. [8, 9]

In the case of S-QSH single helical edge interface, the absence of backscattering channels in the helical edge suppresses NR probability *B(E)* to 0 at all energies. Within the superconducting gap $E < \Delta_S$, electron transmission is excluded, requiring a perfect AR with probability $A(E) = 1$. [14] Evaluating equation (1) in zero temperature limit for this case gives a contact resistance for a single helical edge channel of $h/4e^2$ when $V < \Delta_S/e$. In two-terminal S-QSH-S geometry, used in our experiments, this gives a resistance of each helical edge mode to be $h/4e^2 + h/4e^2 = h/2e^2$, giving a total two-terminal resistance of $h/2e^2 \,||\, h/2e^2 = h/4e^2$. On the other hand, for $E > \Delta_S$ electron transmission into the superconducting lead is possible and AR probability scales as $A(E) \approx \left(\frac{\Delta_S}{E}\right)^2 \to 0$ for $V >> \Delta_S/e$, [23] reducing equation (1) to the familiar case of N-QSH single interface with contact resistance of $h/2e^2$. Simple resistance combination now gives a total two-terminal resistance of $h/2e^2$.

In the present InAs/GaSb QWs this analysis may be somewhat complicated by the presence of residual mini-gap bulk carriers [21, 27] with an estimated carrier density $< 5 \cdot 10^{10}$ cm^{-2}. Such carriers give a background conductance of $G_{bulk} \sim 10e^2/h$, as can be estimated from $g_{bulk} \times (W/L)$, with bulk conductivity $g_{bulk} \sim 5\ e^2/h$. [9] At such low densities, however, apart from significant wavevector mismatch [23, 24], disorder generally dominates and hence a substantial AR contribution from the bulk can be excluded. As a result, AR can be thought as essentially from the edge channels, leading to $\Delta G \equiv G(V=0) - G(V >> \Delta_S / e) = 2e^2/h$ (Fig. 1 inset c). This has indeed been observed (Fig. 2d, $V_{front} = -2.1$V) as a ZBCP of an amplitude $\sim 2e^2/h$, for E_F in the mini-gap. We note that regardless of a high transmissivity of $T = 0.7$ above the mini-gap, in the hybridization regime I-V curve is tunneling like (see Fig. 2e) [25] , which indicates interface transparency of less than 0.5. According to BTK this would give conductance

suppression at zero bias. Because we actually see conductance enhancement, this must be due to edge states and their topological protection. Also, note that the ZBCP is in fact broadened (See Fig. 2d, HWHM ~1.9 meV) in the hybridization gap as compared to outside of the gap (Fig. 2c, HWHM ~ 0.62 meV). A broader than usual ZBCP is in agreement with theoretical prediction of perfect AR on the QSH-S interface. [14] The observation of a ~ $2e^2/h$ AR conductance peak thus renders a strong support for the helical nature of the edge modes.

The I_{excess} deduced in the min-gap shows a large range of fluctuations between 100 to 200 nA; this value is consistent with, but somewhat smaller than, the value obtained from BTK analysis [24]. According to BTK theory, the maximal value of $\frac{e \cdot I_{excess} \cdot R_N}{\Delta_S} = \frac{8}{3}$ at T = 0, for perfectly transmissive interfaces, i.e. when $A = 1$ [26]. In the case of S-QSH-S structures normal resistance is $h/2e^2$ so the maximal excess current that can be obtained for perfectly transmissive helical edge modes with zero backscattering is $I_{excess} = \frac{16}{3}\frac{e \cdot \Delta_S}{h} \sim 250$ nA.

The temperature dependence of I_{excess} in Fig. 3a shows only a weak dependence for temperatures up to 6.5 K, and I_{excess} is quickly suppressed as the temperature is further increased towards the critical temperature of niobium leads. Furthermore, a color map of temperature evolution of dV/dI is shown in Fig. 3b, with dips in dV/dI closely following the BCS temperature dependence of superconducting gap Δ_S. We note here that for both cases, i.e., E_F inside and outside of the mini-gap, I_{excess} show comparative suppression when Δ_S is reduced with increased temperature. This is most easily seen when I_{excess} is normalized by the corresponding low temperature values, i.e. $I_{excess}(T)/ I_{excess}($300 mK$)$ and plotted in Fig. 3c for these two cases.

This is in sharp contrast to the magnetic field dependence of I_{excess} shown in Fig. 4, where I_{excess} for E_F in the mini-gap is suppressed much faster than in the case when E_F is outside of the

mini-gap. In fact, perpendicular magnetic field of less than 50 mT is sufficient to fully suppress AR processes in the mini-gap, while above the mini-gap AR processes survive in fields up to at least 500 mT (Fig. 4a). Similar disparity is also observed for the in-plane magnetic fields, albeit in this case mini-gap I_{excess} survives for fields up to 100 mT while above the mini-gap, AR processes are still observable at 500 mT (Fig. 4b). Such fragility of the observed mini-gap excess current under small magnetic fields is indicative of its origin, namely due to back-scattering protection of helical edge channels under time reversal symmetry. Applying small magnetic fields breaks this symmetry, destroying the perfect destructive interference of back-scattering paths [2], and opening the back-scattering channels in our structures. In this case, maximal AR probability is no longer guaranteed and I_{excess} quickly vanishes. The ZBCP as a function of perpendicular magnetic field in the two cases are shown in Fig. 4c (above the mini-gap) and in Fig. 4d (in the gap), respectively.

In conclusion, we probe the recently discovered helical edge modes in InAs/GaSb QWs via Andreev reflection. A zero bias conductance peak of ~ $2e^2/h$ is observed as the Fermi level is tuned across the mini-gap, which is in good agreement with the prediction of perfect Andreev reflection of the helical edge modes, guaranteed by the absence of back-scattering channels. The perfect AR occurs in spite of a finite barrier at the interface and shows strong sensitivity to time-reversal breaking - hallmarks of helical nature of the QSH edges. With further optimization in fabrication, superconductor-contacted InAs/GaSb system readily arises as a viable platform where theoretical predictions of Majorana fermion bound states [11, 12, 13] can be experimentally explored.

We thank D. C. Tsui, C. Beenakker, M. Wimmer for insightful discussions and comments. The work at Rice was supported by Hackerman Advanced Research Program grant

003604-0062-2009, Welch Foundation grant C-1682, and NSF grant DMR-0706634. IK acknowledges financial assistance of Welch Predoctoral Fellowship.

*Present Address: IBM Almaden Research Center, San Jose, CA 95120

** Electronic Address: rrd@rice.edu

REFERENCES

[1] M. Z. Hasan and C. L. Kane, Rev. Mod. Phys. **82**, 3045(2010).

[2] X.-L. Qi and S.-C. Zhang, Rev. Mod. Phys. **83**, 1057(2011).

[3] L. Fu, and C. L. Kane, Phys. Rev. Lett. **100**, 096407(2008).

[4] C. L. Kane and E. J. Mele, Phys. Rev. Lett. **95**, 226801(2005).

[5] B. A. Bernevig, S. C. Zhang, Phys. Rev. Lett. **96**, 106802(2006).

[6] B. A. Bernevig, T. L. Hughes, S.-C. Zhang, *Science* **314**, 1757(2006).

[7] C. Liu, T. L. Hughes, X.-L. Qi, K. Wang, and S.-C. Zhang, Phys. Rev. Lett., **100**, 236601(2008).

[8] M. Konig, S. Wiedmann, C. Brune, A. Roth, H. Buhmann, L. W. Molenkamp, X.-L. Qi, and S.-C. Zhang, *Science* **318**, 766(2007).

[9] I. Knez, R. R. Du and G. Sullivan, Phys. Rev. Lett., **107**, 136603(2011).

[10] A. Roth, C. Brüne, H. Buhmann, L. W. Molenkamp, J. Maciejko, X.-L. Qi and S.-C. Zhang, *Science* **325**, 294(2009).

[11] J. Nilsson, A. R. Akhmerov, and C. W. Beenakker, Phys. Rev. Lett. **101**, 120403(2008).

[12] L. Fu and C. L. Kane , Phys. Rev. **B 79**, 161408(2009).

[13] C. Benjamin and J. K. Pachos, Phys. Rev. **B 81**, 085101(2010).

[14] P. Adroguer, C. Grenier, D. Carpentier, J. Cayssol, P. Degiovanni, and E. Orignac, Phys. Rev. **B 82**, 081303(R) (2010).

[15] Q.-F. Sun, Y.-X. Li, W. Long, and J. Wang, Phys. Rev. **B 83**, 115315 (2011).

[16] C. Nguyen, J. Werking, H. Kroemer and E. L. Hu, Appl. Phys. Lett. **57**, 87 (1990).

[17] J. P. Heida, B. J. van Wees, T. M. Klapwijk and G. Borghs, Phys. Rev. **B 60**, 13135 (1990).

[18] F. Giazotto, K. Grove-Rasmussen, R. Fazio, F. Beltram, E. H. Linfield and D. A. Ritchie, J. Sup. **17**, 317 (2004).

[19] Y. Naveh and B. Laikhtman, Appl. Phys. Lett. **66**, 1980(1995).

[20] M. Yang, C. Yang, B. Bennett, and B. Shanabrook, Phys. Rev. Lett., **78**, 4613 (1997).

[21] I. Knez, R. R. Du, and G. Sullivan, Phys. Rev. B **81**, 201301(R) (2010).

[22] A. F. Andreev, Zh. Eksp. Teor. Fiz. **46**, 1823 (1964).

[23] G. E. Blonder, M. Tinkham and T. M. Klapwijk, Phys. Rev. **B 25**, 4515 (1982).

[24] We use excess current as a semi-quantitative measure for AR in this experiment. AR probability scales as ratio of superconducting gap to voltage bias squared. Because superconducting gap is ~ 1 meV, a bias of ~ 3mV will significantly suppress AR processes, and hence linear portion is fitted from 3mV to 5mV. This procedure may generally underestimate excess current, but with an error estimated to be less than 10%.

[25] M. Octavio, M. Tinkham, G. E. Blonder and T. M. Klapwijk, Phys. Rev. **B 27**, 6739(1983).

[26] Note that hybridization gap here is only 3 ~ 4 meV in magnitude. Hence by applying several mV we will probe states slightly above and below the center of hybridization gap.

[27] K. Flansberg, J. Bindslev Hansen and M. Octavio, Phys. Rev. **B 38**, 8707 (1988).

[28] Y. Naveh and B. Laikhtman, Euro. Phys. Lett. **55**, 545(2001).

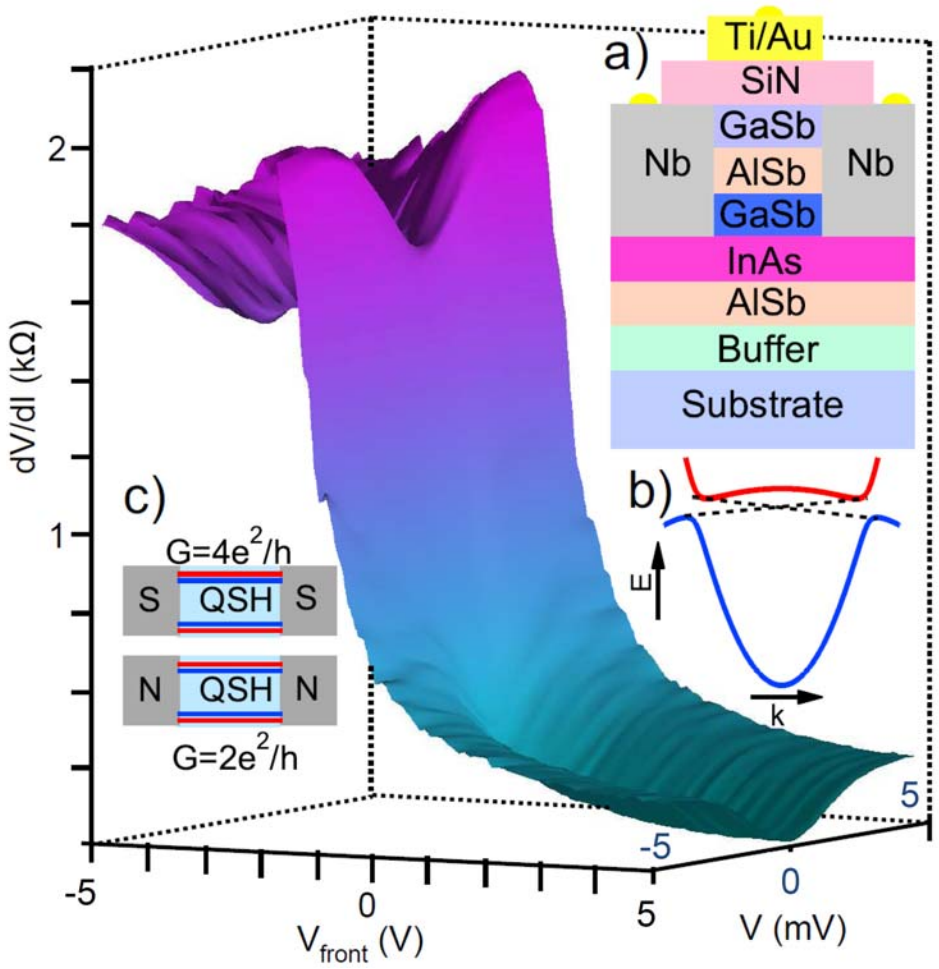

Fig. 1. (Color) Differential resistance *dV/dI* vs bias voltage *V* across the S-InAs/GaSb-S junction as a function of gate bias V_{front} . Inset a) shows device cross-section with Ti/Au front gate on top while inset b) shows energy spectrum of inverted InAs/GaSb QWs with linearly dispersing helical edge modes in the mini-gap. As the Fermi level E_F is tuned across the mini-gap via V_{front}, *dV/dI* exhibits strong peak at larger *V*. On the other hand, for *V* close to zero, *dV/dI* exhibits strong dips, suggesting transport dominated by Andreev reflection processes. Inset c) shows two-terminal structure with superconducting and normal leads. Due to the perfect Andreev reflection

at S-QSH interfaces, voltage drop at each contact is halved, leading to a doubling of differential conductance compared to N-QSH case.

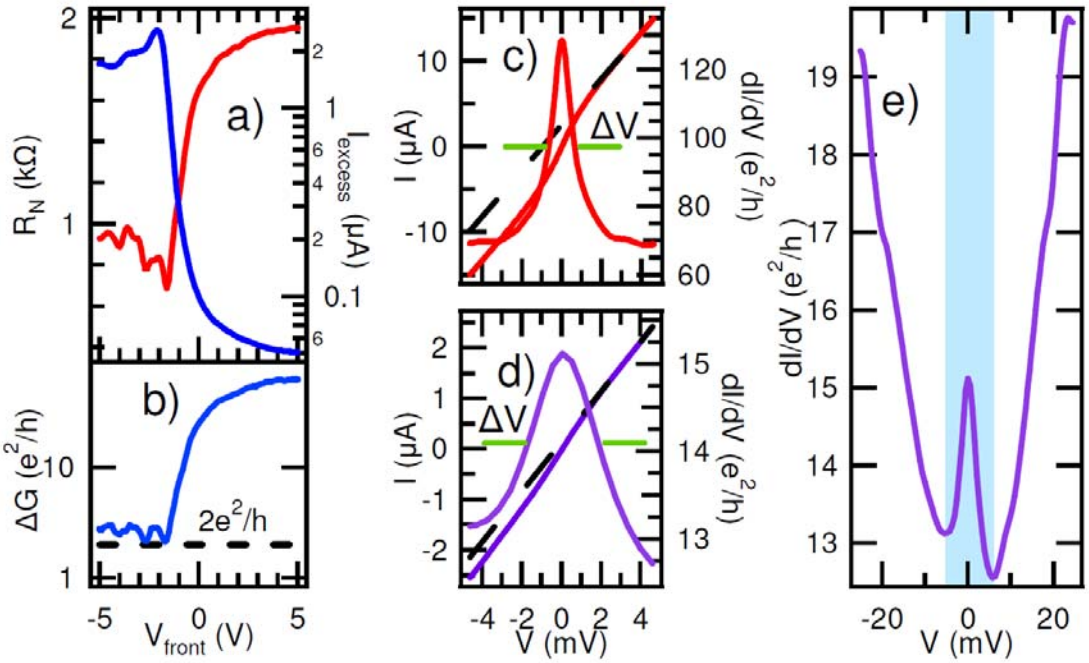

Fig. 2. (Color) Panel a) shows normal resistance R_N (in blue) and excess current due to Andreev reflection I_{excess} (in red) vs V_{front}. As V_{front} is decreased, E_F is tuned towards the mini-gap and R_N increases towards the peak value of ~2kΩ while concurrently I_{excess} decreases from the maximal value of ~2.6 μA (V_{front} = 5 V) to mini-gap value I_{excess} ~150 nA (V_{front} =-2.1V). Panel b) shows conductance difference $\Delta G \equiv G(V=0) - G(V >> \Delta_S / e)$ vs V_{front} on a log scale. For E_F in the mini-gap ΔG shows a plateau at ~ 2.2 e^2/h. Panel c) and d) show zero bias conductance peak (ZBCP) and I vs V for V_{front} = 5V and V_{front} = -2.1 V respectively. Excess current is determined as an intercept of the linear fit to the I-V curve for large V. The ΔV marks FWHM of the respective ZBCP.

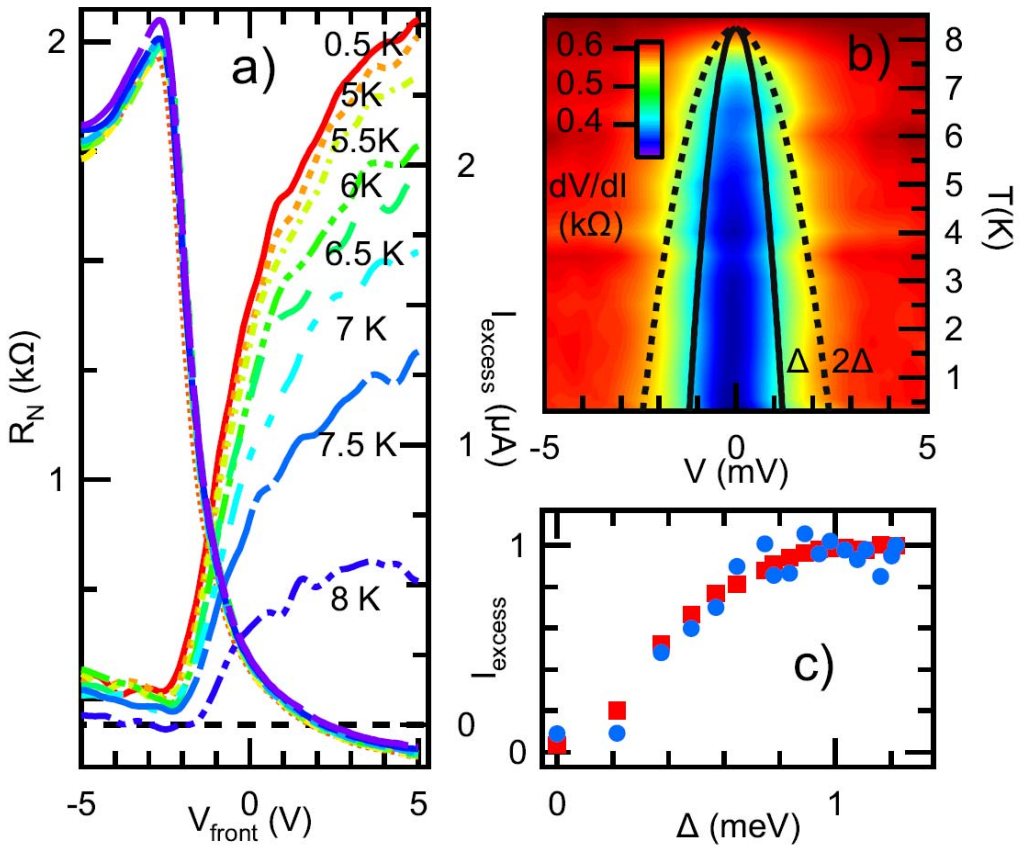

Fig. 3. (Color) Panel a) shows R_N and I_{excess} vs V_{front} for temperature T=0.5 K, and T from 5 K to 8 K varied in 0.5 K increments. Note that I_{excess} drops slowly until the T being close to T_c = 8.27 K. Panel b) shows color map of dV/dI vs V and T (V_{front}=0 V). Full and dashed lines show BCS dependence of the superconducting gap Δ_S/e and $2\Delta_S/e$, respectively. Dips in dV/dI follow closely the BCS gap Δ_S. Panel c) shows normalized I_{excess}, i.e. $I_{excess}(T)/ I_{excess}$(300 mK), vs $\Delta_S(T)$ for E_F above the mini-gap (in red) and E_F in the mini-gap (in blue). In both cases, normalized I_{excess} shows equal decrease as the Δ_S is reduced with T.

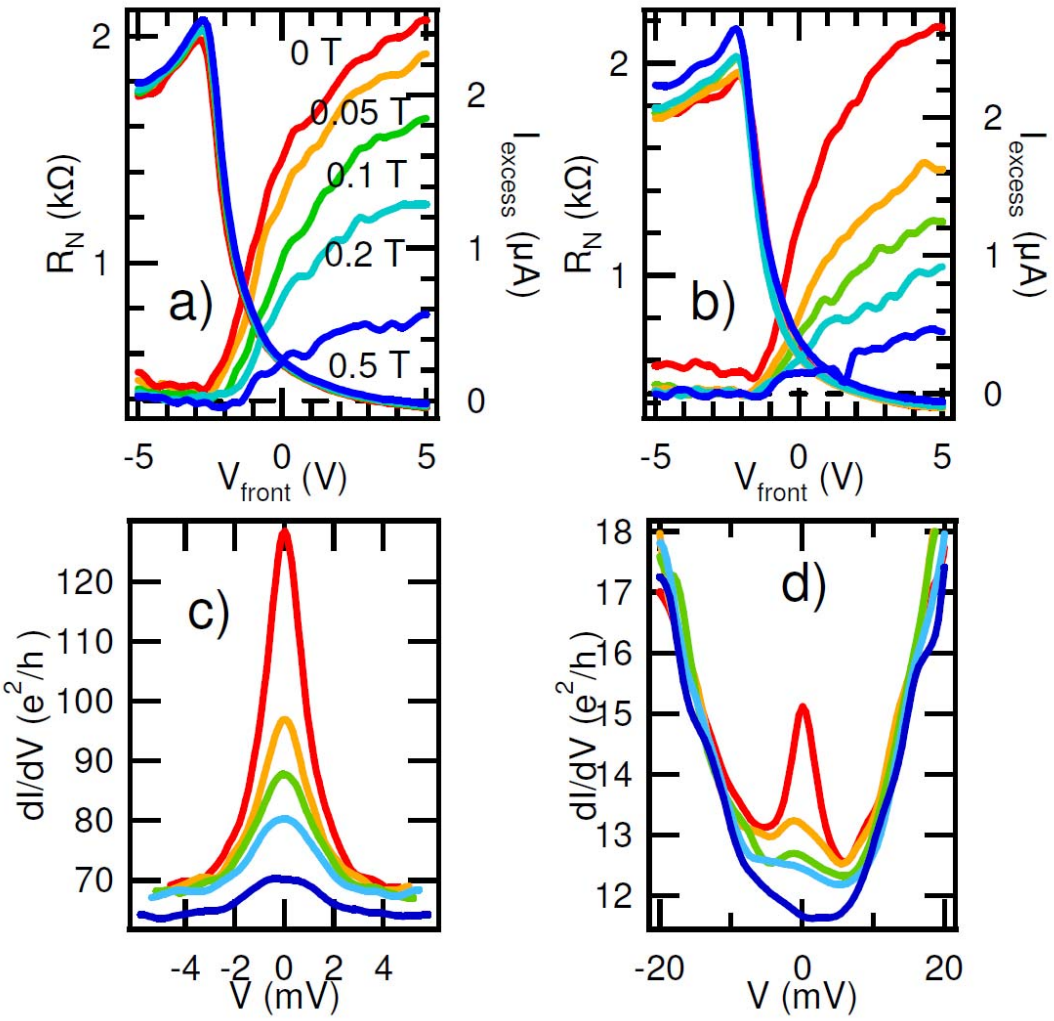

Fig. 4. (Color) Panel a) shows R_N and I_{excess} vs V_{front} for perpendicular magnetic fields of B_{perp} = 0, 0.05, 0.1, 0.2, and 0.5 T, and panel b) for in-plane magnetic fields $B_{||}$ with the same increments. The $B_{||}$ axis is approximately 45° with respect to the junction interfaces. Although for E_F above the hybridization gap, I_{excess} survives up to 0.5 T, for E_F in the mini-gap I_{excess} is completely suppressed with B_{perp} = 0.05 T or $B_{||}$= 0.1 T. This is in contrast to the equal suppression of I_{excess} in temperature dependence (Fig. 3c), suggesting different nature of excess current within and outside of the hybridization gap. Panels c) and d) show respectively the ZBCP for E_F above the mini-gap, or in the gap, for perpendicular magnetic fields corresponding to a).